


RESEARCH ARTICLE | MARCH 10 2026

Formation process and composition-dependent properties in non-centrosymmetric Ta₂O₅ phase with Zr substitution

Suzuka Udagawa ; Takanori Mimura  ; Tetsuhiro Katsumata ; Yoshitaka Matsushita ; Takashi Mochiku ; Yoshiyuki Inaguma 



J. Appl. Phys. 139, 104102 (2026)

<https://doi.org/10.1063/5.0312634>



View
Online



Export
Citation

Articles You May Be Interested In

A dielectric material, Zr_{0.10}Ta_{0.90}O_{2.45}, with a noncentrosymmetric L-Ta₂O₅-related structure

Appl. Phys. Lett. (April 2025)

Plasmonic spectral tunability of conductive ternary nitrides

Appl. Phys. Lett. (June 2016)

Growth and dielectric properties of Ta₂O₅ single crystal fibers

PICALO2008



 Zurich
Instruments

Freedom to Innovate.

The New VHFLI 200 MHz Lock-in Amplifier.

Orchestrate pulses, triggers, and acquisition as the hub of your experiment.
Discover more – run every signal analysis tool, simultaneously.

Order now

Formation process and composition-dependent properties in non-centrosymmetric Ta₂O₅ phase with Zr substitution

Cite as: J. Appl. Phys. 139, 104102 (2026); doi: 10.1063/5.0312634

Submitted: 18 November 2025 · Accepted: 23 February 2026 ·

Published Online: 10 March 2026



Suzuka Udagawa,¹ Takanori Mimura,^{1,a)} Tetsuhiro Katsumata,² Yoshitaka Matsushita,³ Takashi Mochiku,³ and Yoshiyuki Inaguma^{1,b)}

AFFILIATIONS

¹Department of Chemistry, Faculty of Science, Gakushuin University, 1-5-1 Mejiro, Toshima-ku, Tokyo 171-8588, Japan

²Department of Chemistry, School of Science, Tokai University, 4-1-1 Kitakaname, Hiratsuka, Kanagawa 259-1292, Japan

³Research Network and Facility Services Division, National Institute for Materials Science (NIMS), 1-2-1 Sengen, Tsukuba, Ibaraki 305-0047, Japan

^{a)}Author to whom correspondence should be addressed: 20220185@gakushuin.ac.jp

^{b)}Email: yoshiyuki.inaguma@gakushuin.ac.jp

ABSTRACT

(Zr_xTa_{1-x})₂O_{5-x} was prepared by a solid-state reaction of ZrO₂ and Ta₂O₅, and the L'-Ta₂O₅ phase was obtained by cooling the H-Ta₂O₅ phase. High-temperature x-ray diffraction measurements showed that the starting materials, ZrO₂ and low-temperature L-Ta₂O₅, formed the high-temperature H-Ta₂O₅ phase when heated above 1360 °C. Upon cooling, this phase sequentially transformed into L''-Ta₂O₅, the high-temperature L'-Ta₂O₅ phase, and L-Ta₂O₅ phases. As the Zr content, *x*, decreased, the transition from the H-Ta₂O₅ phase to the L''-Ta₂O₅ phase slowed. The temperature dependence of the dielectric constant revealed a maximum value, which is attributed to the phase transition from L'-Ta₂O₅ to L''-Ta₂O₅. This transition temperature decreases by approximately 50 °C for every 0.01 increase in the *x* value. The L'-Ta₂O₅ phase exhibited negative volumetric thermal expansion (NTE) behavior near the phase transition temperature. As *x* decreased, the NTE coefficient increased from $-1.09 \times 10^{-6}/\text{K}$ (77–127 °C) for *x* = 0.10 to $-2.06 \times 10^{-5}/\text{K}$ (327–427 °C) for *x* = 0.05. The substitution of Zr into Ta₂O₅ stabilized the non-centrosymmetric L'-Ta₂O₅ phase and controlled the phase transition temperature and thermal expansion behavior.

© 2026 Author(s). All article content, except where otherwise noted, is licensed under a Creative Commons Attribution (CC BY) license (<https://creativecommons.org/licenses/by/4.0/>). <https://doi.org/10.1063/5.0312634>

I. INTRODUCTION

Dielectric materials are essential to a wide variety of technologies, including microelectronics, medical devices, and energy storage systems.^{1–6} Ta₂O₅ is a significant dielectric material recognized for its high dielectric constant, nonlinear refractive index, and wide bandgap.⁷ Therefore, it is used in dynamic random-access memory (DRAM) applications and antireflection coatings.^{8,9}

Ta₂O₅ exists primarily in two different phases based on the temperature: the high-temperature H-Ta₂O₅ phase and the low-temperature L-Ta₂O₅ phase, with a phase transformation occurring at *T* = 1360 °C.¹⁰ This transformation is reversible and occurs slowly; annealing below 1360 °C and/or slow cooling effectively

facilitates the transition from the H-Ta₂O₅ phase to the L-Ta₂O₅ phase.^{10–12} These two phases have complex structures with various reported crystal structures. For the H-Ta₂O₅ phase, the proposed space groups include *I*2, *Imma*, *C2/m*, and *I*4₁/*amd*, while for the L-Ta₂O₅ phase, *Pmm*2, *Pccm*, and *P2mm* have been suggested. The tetragonal *I*4₁/*amd* structure (*a* = 3.86 Å and *c* = 36.18 Å) is widely accepted for the H-Ta₂O₅ phase, whereas the orthorhombic *P2mm* structure (*a* = 6.198 Å, *b* = 40.290 Å, and *c* = 3.888 Å) is for the L-Ta₂O₅ phase.^{12,13}

Cation substitution can change the crystal structure and physical properties in Ta₂O₅-based materials. The compounds (Si_xTa_{1-x})₂O_{5-x} form the L-Ta₂O₅ phase for *x* = 0.00–0.11, which

12 March 2026 00:17:58

has a dielectric constant of ~ 30 .¹⁴ By contrast, $(\text{Zr}_x\text{Ta}_{1-x})_2\text{O}_{5-x}$ can form either the $\text{L-Ta}_2\text{O}_5$ or $\text{H-Ta}_2\text{O}_5$ phase for $x=0.00\text{--}0.14$, depending on heating conditions, exhibiting dielectric constants of roughly 30 and 50, respectively.¹⁵ For $(\text{Ti}_x\text{Ta}_{1-x})_2\text{O}_{5-x}$, the $\text{H-Ta}_2\text{O}_5$ phase forms within the composition range of $x=0.0\text{--}0.25$, corresponding to dielectric constants of 20–126 depending on substitution concentrations.^{16,17} Notably, $(\text{Ti}_{0.04}\text{Ta}_{0.96})_2\text{O}_{4.96}$ shows a high dielectric constant of 126 owing to structural distortion.^{17,18}

Recently, we identified a new dielectric material, refined as the $\text{L}'\text{-Ta}_2\text{O}_5$ phase, in $(\text{Zr}_{0.10}\text{Ta}_{0.90})_2\text{O}_{4.90}$, which was synthesized by heating a mixture of Ta_2O_5 and ZrO_2 powders at 1700°C for 10 h.¹⁹ This material has a C-centered orthorhombic structure ($a=6.3717\text{ \AA}$, $b=10.8003\text{ \AA}$, and $c=3.87058\text{ \AA}$) related to the $\text{L-Ta}_2\text{O}_5$ structure. The $\text{L}'\text{-Ta}_2\text{O}_5$ phase exhibits a strong second-harmonic generation (SHG) signal, which is not present in the conventional $\text{L-Ta}_2\text{O}_5$ phase. It also shows a higher dielectric constant of ~ 55 , compared with 33 for the $\text{L-Ta}_2\text{O}_5$ phase fired at 1200°C for 10 h. Moreover, high-temperature x-ray diffraction (HTXRD) measurements revealed the high-temperature $\text{L}'\text{-Ta}_2\text{O}_5$ phase, which has a pseudo-hexagonal structure. The dielectric constant depends on temperature and exhibits a maximum value of 60 at 87°C , corresponding to this phase transition. These findings indicate the potential of $\text{L}'\text{-Ta}_2\text{O}_5$ as a new non-centrosymmetric dielectric material. As it stands, the $\text{L}'\text{-Ta}_2\text{O}_5$ phase has only been synthesized for the specific composition of $(\text{Zr}_{0.10}\text{Ta}_{0.90})_2\text{O}_{4.90}$; no research has been conducted on the synthesis and characterization of other compositions within the $(\text{Zr}_x\text{Ta}_{1-x})_2\text{O}_{5-x}$ family. Moreover, why heating at 1700°C results in the formation of the $\text{L}'\text{-Ta}_2\text{O}_5$ phase instead of the previously observed $\text{L-Ta}_2\text{O}_5$ or $\text{H-Ta}_2\text{O}_5$ phases in $(\text{Zr}_x\text{Ta}_{1-x})_2\text{O}_{5-x}$ systems remains unclear.

In this work, we investigated the composition range that leads to the formation of the $\text{L}'\text{-Ta}_2\text{O}_5$ phase within the $(\text{Zr}_x\text{Ta}_{1-x})_2\text{O}_{5-x}$ system. We found that a pure $\text{L}'\text{-Ta}_2\text{O}_5$ phase formed in the composition range of $x=0.05\text{--}0.11$ by optimizing the heat-treatment conditions. To investigate the formation pathway of the $\text{L}'\text{-Ta}_2\text{O}_5$ phase from the starting materials, ZrO_2 and $\text{L-Ta}_2\text{O}_5$, we conducted HTXRD measurements. We report the formation process and composition-dependent properties of non-centrosymmetric $\text{L}'\text{-Ta}_2\text{O}_5$ type $(\text{Zr}_x\text{Ta}_{1-x})_2\text{O}_{5-x}$.

II. EXPERIMENTAL

$(\text{Zr}_x\text{Ta}_{1-x})_2\text{O}_{5-x}$ ($x=0.04\text{--}0.13$) was synthesized via a solid-state reaction using ZrO_2 (rare metallic, $>99.99\%$ purity, $<2\%$ Hf) and Ta_2O_5 (rare metallic, $>99.99\%$ purity, low-temperature $\text{L-Ta}_2\text{O}_5$) powders as starting materials in a stoichiometric ratio. The powders were mixed with ethanol using an agate mortar, then dried at 120°C , and pressed into $\phi 7\text{ mm}$ or $\phi 10\text{ mm}$ pellets. These pellets were sintered at 1700°C for either 10 or 5 h at a heating rate of $2.6^\circ\text{C}/\text{min}$ and cooling rate of $1.2^\circ\text{C}/\text{min}$. Subsequently, the pellets were heated at 1200°C for 10 h. In both heating processes, the pellets were heated in air. XRD measurements were performed for phase identification using a PANalytical X'Pert³ powder diffractometer ($\text{Cu K}\alpha$, $\lambda=0.15418\text{ nm}$). To investigate the formation process of the $\text{L}'\text{-Ta}_2\text{O}_5$ phase, *in situ* HTXRD measurements were performed over a temperature range of $28\text{--}1450^\circ\text{C}$ using a Bruker AXS D8 ADVANCE diffractometer

equipped with a high-temperature stage ($\text{Cu K}\alpha$, $\lambda=0.15418\text{ nm}$). The starting material consisted of a mixture of ZrO_2 and $\text{L-Ta}_2\text{O}_5$ powders in a stoichiometric ratio corresponding to $(\text{Zr}_{0.10}\text{Ta}_{0.90})_2\text{O}_{4.90}$. The sample was placed on a Pt heater and directly heated under a nitrogen atmosphere. Synchrotron powder XRD was conducted for the sample with $x=0.05$ from -173 to 800°C using Debye-Scherrer-type powder diffractometer at SPring-8 (BL13XU, $\lambda=0.375695\text{ nm}$). The sample powder was packed into a quartz glass capillary with an outer diameter of 0.1 mm and a wall thickness of 0.01 mm .

SHG measurements were performed at room temperature to confirm the non-centrosymmetry. A modified Kurtz nonlinear optical (NLO) system using 1064 nm light ($\text{Nd}:\text{YAG}$ laser) was used for the SHG measurement.²⁰ To measure the dielectric constant, $\phi 7\text{ mm}$ gold electrodes were deposited on both sides of the pellets using a direct-current sputtering method. The dielectric constant was measured using an inductance-capacitance-resistance (LCR) meter (4284A; Agilent, Palo Alto, CA, USA) at frequencies of 1 kHz , 10 kHz , 50 kHz , 100 kHz , 200 kHz , 500 kHz , and 1 MHz with an applied signal of 1 V in the temperature range of $30\text{--}370^\circ\text{C}$ in air.

III. OPTIMIZING THE HEATING CONDITIONS TO FORM THE $\text{L}'\text{-Ta}_2\text{O}_5$ PHASE IN $(\text{Zr}_x\text{Ta}_{1-x})_2\text{O}_{5-x}$ FOR $x=0.05\text{--}0.11$

Figure 1 shows the XRD patterns of $(\text{Zr}_x\text{Ta}_{1-x})_2\text{O}_{5-x}$ ($x=0.04\text{--}0.13$) obtained by heating at 1700°C . The reference pattern for the $\text{L-Ta}_2\text{O}_5$ phase ($P2mm$) is included for comparison.¹³ For the compositions with $x=0.06\text{--}0.13$, the two prominent peaks around $2\theta=28^\circ$ were inverted in relation to the peak intensities of the $\text{L-Ta}_2\text{O}_5$ phase. This inversion indicates the formation of the $\text{L}'\text{-Ta}_2\text{O}_5$ phase. Among these compositions, the samples with $x=0.09\text{--}0.11$ formed a single $\text{L}'\text{-Ta}_2\text{O}_5$ phase without any impurity phases. However, the $\text{Zr}_6\text{Ta}_2\text{O}_{17}$ phase was observed as an impurity in the samples with $x=0.12\text{--}0.13$. Note that the $\text{Zr}_6\text{Ta}_2\text{O}_{17}$ phase remained even after re-heating at 1700°C for 10 h (not shown here). Therefore, the solid-solution limit of ZrO_2 to Ta_2O_5 was estimated to be $x=0.11$ in $(\text{Zr}_x\text{Ta}_{1-x})_2\text{O}_{5-x}$. For compositions with $x=0.05\text{--}0.08$, the $\text{H-Ta}_2\text{O}_5$ phase was formed. The weight fraction of the $\text{H-Ta}_2\text{O}_5$ phase relative to the $\text{L}'\text{-Ta}_2\text{O}_5$ phase increased with decreasing ZrO_2 substitution, and only the $\text{H-Ta}_2\text{O}_5$ phase was obtained for the samples with $x=0.04\text{--}0.05$.

Based on the binary phase diagram of Ta_2O_5 and ZrO_2 , the $\text{H-Ta}_2\text{O}_5$ phase is formed at 1700°C during heating.^{15,21} This indicates that the $\text{L}'\text{-Ta}_2\text{O}_5$ phase is formed by cooling the $\text{H-Ta}_2\text{O}_5$ phase. Additionally, the $\text{L}'\text{-Ta}_2\text{O}_5$ phase has a high-temperature $\text{L}''\text{-Ta}_2\text{O}_5$ phase, as mentioned in a previous report.¹⁹ Therefore, the phase transitions during cooling are expected to proceed as $\text{H-Ta}_2\text{O}_5 \rightarrow \text{L}''\text{-Ta}_2\text{O}_5 \rightarrow \text{L}'\text{-Ta}_2\text{O}_5$, as illustrated in Fig. S1(a) in the supplementary material.

The transformation from the $\text{H-Ta}_2\text{O}_5$ phase to the conventional $\text{L-Ta}_2\text{O}_5$ phase is sluggish; therefore, the phase transition to the $\text{L}''\text{-Ta}_2\text{O}_5$ phase is also expected to be slow.^{10–12} For compositions with $x=0.04\text{--}0.08$, the $\text{H-Ta}_2\text{O}_5$ phase could be fully or partially quenched to room temperature, even with a slow furnace cooling rate of $1.2^\circ\text{C}/\text{min}$. This indicates that the activation energy

12 March 2026 00:17:58

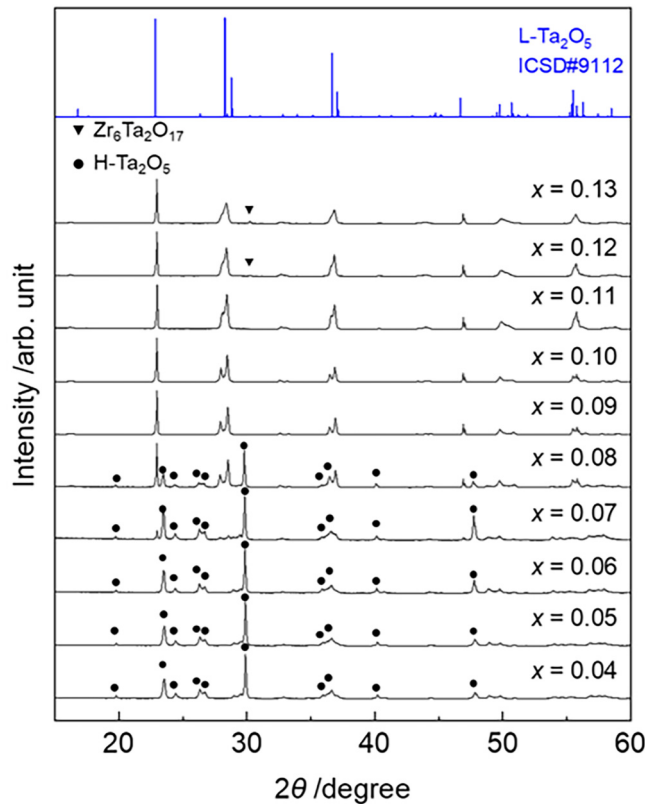


FIG. 1. XRD patterns of $(\text{Zr}_x\text{Ta}_{1-x})_2\text{O}_{5-x}$ heated at 1700°C for 10 h, with a reference pattern of $\text{L-Ta}_2\text{O}_5$ ($P2mm$, ICSD No. 9112). The filled circles and triangles represent reflections from the $\text{H-Ta}_2\text{O}_5$ phase and $\text{Zr}_6\text{Ta}_2\text{O}_{17}$, respectively.

barrier required for the transition from the $\text{H-Ta}_2\text{O}_5$ phase to the $\text{L}''\text{-Ta}_2\text{O}_5$ phase is relatively high in this composition region. To promote this phase transition, either slowing the cooling rate further or implementing an additional annealing process is necessary, as shown in Figs. S1(a) and S1(b) in the [supplementary material](#).

To produce the $\text{L}'\text{-Ta}_2\text{O}_5$ phase, samples of $x = 0.04\text{--}0.08$, which initially formed the $\text{H-Ta}_2\text{O}_5$ phase when heated at 1700°C for 10 h, were subsequently heated at 1200°C for 10 h. This temperature was chosen because it is slightly lower than the stabilization point of the $\text{H-Ta}_2\text{O}_5$ phase at 1360°C and is expected to promote the phase transition to the $\text{L}'\text{-Ta}_2\text{O}_5$ phase. Figure 2 displays the XRD patterns of $(\text{Zr}_x\text{Ta}_{1-x})_2\text{O}_{5-x}$ ($x = 0.04\text{--}0.08$) after re-heating. The two prominent peaks around $2\theta = 28^\circ$ were inverted, indicating the formation of the $\text{L}'\text{-Ta}_2\text{O}_5$ phase. A pure $\text{L}'\text{-Ta}_2\text{O}_5$ phase was obtained for samples with $x = 0.05\text{--}0.08$, whereas an additional impurity $\text{L-Ta}_2\text{O}_5$ phase was formed for $x = 0.04$. Based on Figs. 1 and 2, a single $\text{L}'\text{-Ta}_2\text{O}_5$ phase was confirmed for the samples with $x = 0.05\text{--}0.11$. Moreover, the SHG responses observed for these compositions support the formation

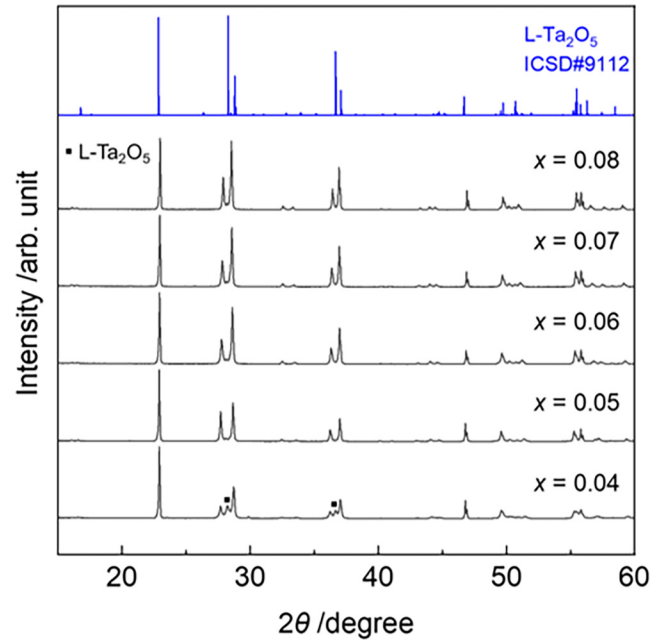


FIG. 2. XRD patterns of $(\text{Zr}_x\text{Ta}_{1-x})_2\text{O}_{5-x}$ heated at 1700°C for 10 h, followed by additional heating at 1200°C for 10 h. Reference pattern is $\text{L-Ta}_2\text{O}_5$ with a $P2mm$ structure (ICSD No. 9112). The filled squares indicate reflections from the $\text{L-Ta}_2\text{O}_5$ phase.

of the $\text{L}'\text{-Ta}_2\text{O}_5$ phase, as shown in Fig. S2 in the [supplementary material](#).

IV. FORMATION PROCESS OF THE $\text{L}'\text{-Ta}_2\text{O}_5$ PHASE CONFIRMED BY HTXRD MEASUREMENT

The expected formation sequence of the $\text{L}'\text{-Ta}_2\text{O}_5$ phase, illustrated in Figs. S1(a) and S1(b) in the [supplementary material](#), begins with a mixture of ZrO_2 and Ta_2O_5 as the starting materials. Upon heating, this mixture transforms into a solid solution of the high-temperature $\text{H-Ta}_2\text{O}_5$ phase.^{15,21} As it cools, it transforms into the $\text{L}''\text{-Ta}_2\text{O}_5$ phase, followed by a transition to the $\text{L}'\text{-Ta}_2\text{O}_5$ phase.¹⁹

To verify this expected formation process, HTXRD analysis was conducted according to the pathway outlined in Fig. S1(b) in the [supplementary material](#). ZrO_2 and Ta_2O_5 powders mixed in a stoichiometric ratio corresponding to $(\text{Zr}_{0.10}\text{Ta}_{0.90})_2\text{O}_{4.90}$ were used as the starting materials. The whole time series of the HTXRD results is shown in Fig. 3 as a 3D diagram. The horizontal and vertical axes represent the 2θ angle and time, respectively, while the temperature at each time point is drawn on the right. Yellow dashed lines separate the obtained phases at each time scale. Reference patterns for the $\text{L-Ta}_2\text{O}_5$ phase ($P2mm$) and $\text{H-Ta}_2\text{O}_5$ phase ($I4_1/amd$) are also included in the figure above. Figure S3 in the [supplementary material](#) presents the raw XRD data collected at each measurement step.

12 March 2026 00:17:58

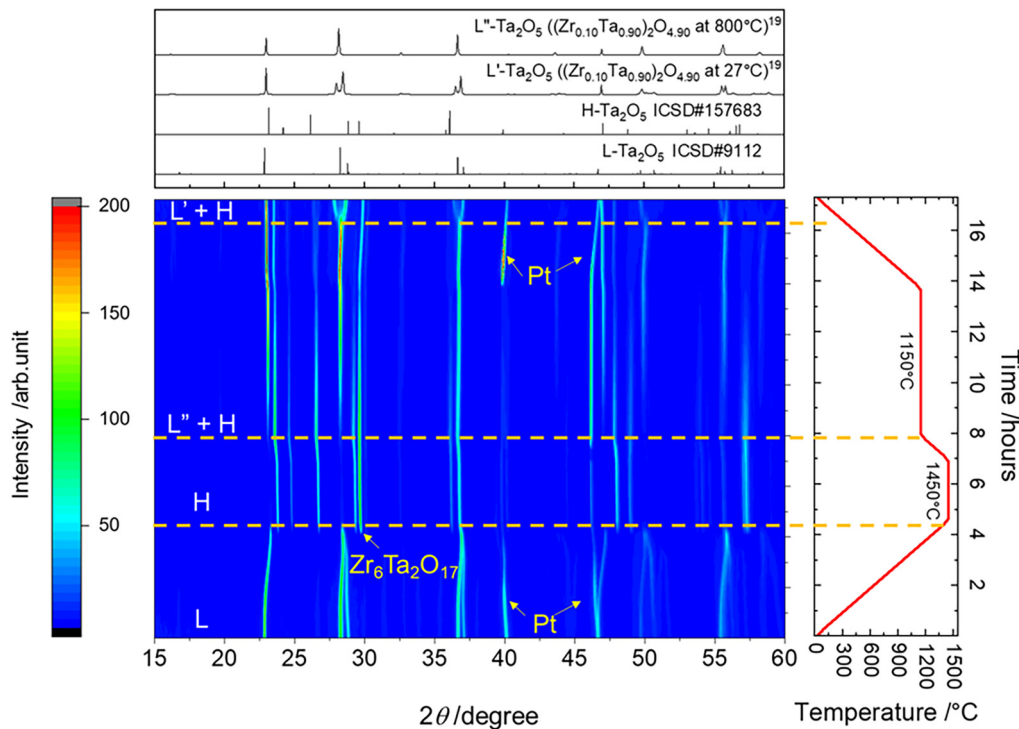


FIG. 3. HTXRD patterns of a sample consisting of mixed Ta_2O_5 and ZrO_2 powders as a function of the temperature in the range of 28–1450 °C. The lower-right figure indicates the temperature profile as a function of time during the measurement. The upper figure is the reference diffraction patterns of $\text{L}'\text{-Ta}_2\text{O}_5$ (ICSD No. 9112), $\text{H-Ta}_2\text{O}_5$ (ICSD No. 157683), $\text{L}'\text{-Ta}_2\text{O}_5[(\text{Zr}_{0.10}\text{Ta}_{0.90})_2\text{O}_{4.90}]$ measured at 27 °C¹⁹, and $\text{L}''\text{-Ta}_2\text{O}_5[(\text{Zr}_{0.10}\text{Ta}_{0.90})_2\text{O}_{4.90}]$ measured at 800 °C¹⁹. The diffraction peaks observed near $2\theta = 40^\circ$ and 45° originate from the Pt heater used during the measurement.

At room temperature, the observed XRD peaks were those of starting materials of ZrO_2 and Ta_2O_5 . With an increase in temperature, the peak from ZrO_2 observed at $2\theta = 31.5^\circ$ disappeared at 1200 °C, indicating that ZrO_2 was dissolved in Ta_2O_5 as shown in Fig. S4 in the [supplementary material](#). This dissolution resulted in a change in the diffraction peak positions of the $\text{L-Ta}_2\text{O}_5$ phase. Additionally, a small amount of the impurity $\text{Zr}_6\text{Ta}_2\text{O}_{17}$ phase formed, as shown in Fig. 3. This $\text{Zr}_6\text{Ta}_2\text{O}_{17}$ phase remained even after the HTXRD measurements were completed.

The binary phase diagram of $(\text{Zr}_x\text{Ta}_{1-x})_2\text{O}_{5-x}$ at $x = 0.10$ and 1200 °C reveals the phase segregation of $\text{L-Ta}_2\text{O}_5$ (Zr-substituted $\text{L-Ta}_2\text{O}_5$) and $\text{Zr}_6\text{Ta}_2\text{O}_{17}$,²¹ which is consistent with our results. Although this phase diagram describes the $\text{L-Ta}_2\text{O}_5$ phase, the XRD peak at 1200 °C closely resembles the $\text{L}''\text{-Ta}_2\text{O}_5$ phase, as the gap between the two diffraction peaks around $2\theta = 28^\circ$ narrowed and merged into a single peak. However, the $\text{L}'\text{-Ta}_2\text{O}_5$ phase did not form after 1200 °C heat treatment for 10 h, confirming its identity as the $\text{L-Ta}_2\text{O}_5$ phase. The transition from the $\text{L-Ta}_2\text{O}_5$ to $\text{H-Ta}_2\text{O}_5$ phase was confirmed at 1400 °C, aligning with a previous report that this phase forms above 1360 °C.¹⁰ The $\text{H-Ta}_2\text{O}_5$ phase remained the main phase when the temperature was held at 1450 °C and subsequently decreased to 1150 °C.

During the holding process at 1150 °C, peaks corresponding to the $\text{L}''\text{-Ta}_2\text{O}_5$ phase emerged. With increasing holding time, the peak intensity increased, while the peak intensity of the $\text{H-Ta}_2\text{O}_5$ phase decreased. This observation indicates that the $\text{H-Ta}_2\text{O}_5$ phase gradually changed into the $\text{L}''\text{-Ta}_2\text{O}_5$ phase. After holding at 1150 °C for 5 h, the $\text{L}''\text{-Ta}_2\text{O}_5$ phase became the main phase. However, the $\text{H-Ta}_2\text{O}_5$ phase remained, indicating that the phase transition was incomplete owing to the limited holding time. Upon cooling to 30 °C, peaks corresponding to the $\text{L}'\text{-Ta}_2\text{O}_5$ phase emerged at 200 °C, indicating a transition from the $\text{L}''\text{-Ta}_2\text{O}_5$ phase to the $\text{L}'\text{-Ta}_2\text{O}_5$ phase. Notably, the phase transition temperature observed here differs from that reported previously (ca. 400 K, 127 °C), estimated from the observable change in the XRD peak pattern of HTXRD measurement.¹⁹ This discrepancy can be attributed to the fact that the amount of Zr in the composition of $\text{L}'\text{-Ta}_2\text{O}_5$ is lower than in $(\text{Zr}_{0.10}\text{Ta}_{0.90})_2\text{O}_{4.90}$ owing to the formation of $\text{Zr}_6\text{Ta}_2\text{O}_{17}$, as shown in Fig. 3. The correlation between Zr substitution content and phase transition temperature will be discussed later.

For compositions with $x = 0.09\text{--}0.11$, the single $\text{L}'\text{-Ta}_2\text{O}_5$ phase was achieved by heating at 1700 °C for 10 h, while for compositions with $x = 0.05\text{--}0.08$, both the $\text{L}'\text{-Ta}_2\text{O}_5$ phase and impurity

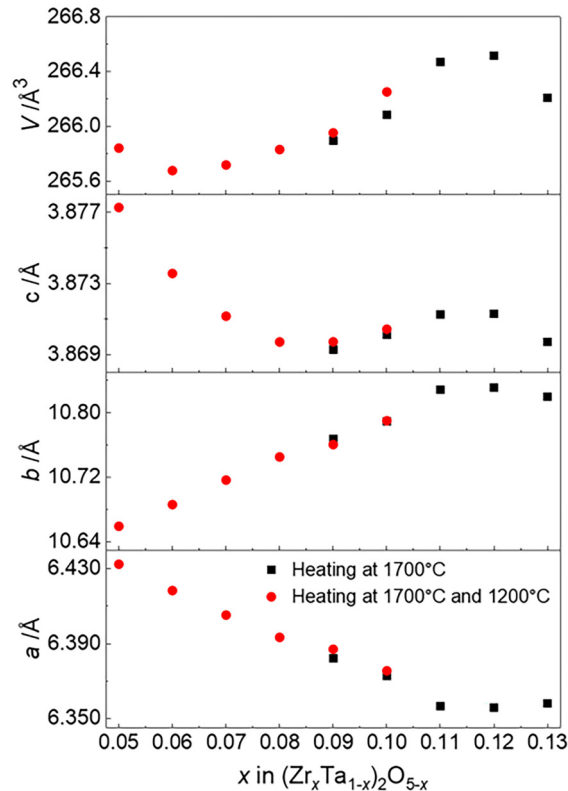


FIG. 4. Compositional dependence of the unit-cell volume and lattice parameters for $(\text{Zr}_x\text{Ta}_{1-x})_2\text{O}_{5-x}$ ($x=0.05\text{--}0.13$). Filled red circles represent data obtained from samples subjected to sequential heating at 1700°C followed by 1200°C . Filled black squares represent data from samples heated only at 1700°C .

$\text{H-Ta}_2\text{O}_5$ phase were obtained, as shown in Fig. 1. According to the HTXRD measurement, the $\text{L}'\text{-Ta}_2\text{O}_5$ phase forms through a sequence of phase transitions during cooling: first from the $\text{H-Ta}_2\text{O}_5$ phase to the $\text{L}''\text{-Ta}_2\text{O}_5$ phase and then from the $\text{L}''\text{-Ta}_2\text{O}_5$ phase to the $\text{L}'\text{-Ta}_2\text{O}_5$ phase. Notably, if the $\text{H-Ta}_2\text{O}_5$ phase cannot transition into the $\text{L}''\text{-Ta}_2\text{O}_5$ phase at high temperatures, it is quenched to room temperature. Therefore, the formation of the $\text{H-Ta}_2\text{O}_5$ phase for $x=0.05\text{--}0.08$ might be derived from the incomplete phase transition to the $\text{L}''\text{-Ta}_2\text{O}_5$ phase. This phase transition is kinetically controlled, as indicated by the requirement for a constant holding time of 1150°C to complete the transition. The peak intensity of the $\text{H-Ta}_2\text{O}_5$ phase increases with decreasing ZrO_2 content, indicating that the transition of the $\text{H-Ta}_2\text{O}_5$ phase into the $\text{L}''\text{-Ta}_2\text{O}_5$ phase slows with decreasing Zr content. In other words, a lower Zr content leads to a higher activation barrier for this phase transition. Therefore, additional heat treatment is required to overcome this activation barrier to obtain the $\text{L}'\text{-Ta}_2\text{O}_5$ phase for the compositions with $x=0.05\text{--}0.08$, as shown in Fig. 2.

V. COMPOSITIONAL DEPENDENCE OF THE PHYSICAL PROPERTIES

A. Lattice parameters

The lattice parameters of the $\text{L}'\text{-Ta}_2\text{O}_5$ phase for $x=0.05\text{--}0.13$ were refined using the Le Bail method.²² Figure 4 shows the compositional dependence of the lattice parameters. All data values including errors are shown in Table S1 in the [supplementary material](#). The lattice parameters exhibit an increase in a and a decrease in b as the amount of ZrO_2 substitution increases within the range $x=0.05\text{--}0.11$, where the $\text{L}'\text{-Ta}_2\text{O}_5$ phase is observed as a single phase. Moreover, c decreases in the composition range of $x=0.05\text{--}0.08$, while it remains nearly constant between $x=0.08$ and 0.11 . The unit-cell volume also decreased upon increasing x from 0.05 to 0.06 , followed by an increase when x was raised from

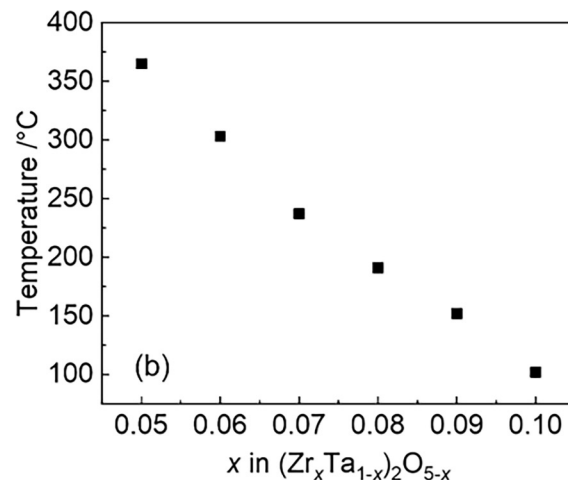
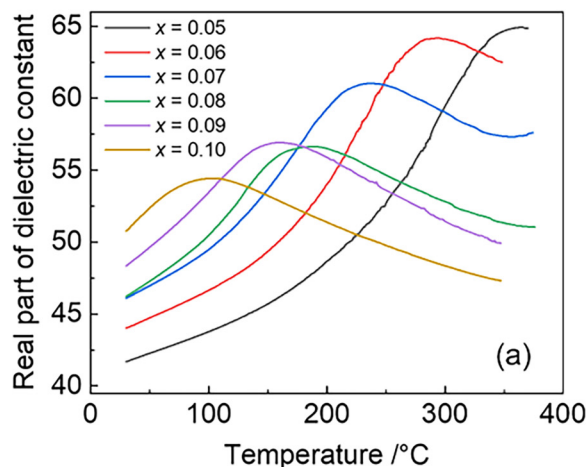


FIG. 5. (a) Compositional and temperature dependence of real part of dielectric constant of $(\text{Zr}_x\text{Ta}_{1-x})_2\text{O}_{5-x}$ ($x=0.05\text{--}0.10$) measured at 1 MHz . (b) Compositional dependence of phase transition temperature between $\text{L}'\text{-Ta}_2\text{O}_5$ and $\text{L}''\text{-Ta}_2\text{O}_5$ for $(\text{Zr}_x\text{Ta}_{1-x})_2\text{O}_{5-x}$ ($x=0.05\text{--}0.10$).

12 March 2026 00:17:58

0.08 to 0.11. At $x=0.12$ – 0.13 , where the impurity $\text{Zr}_6\text{Ta}_2\text{O}_{17}$ is produced as shown in Fig. 1, a and b remain constant, while c increases. These variations in lattice parameters would be derived from not only the Zr substitution effect but also the formation of oxygen vacancies. However, a comprehensive structural analysis of each composition has not been conducted. A detailed structural determination by neutron diffraction measurements will reveal these specific changes in the future.

B. Dielectric constant

Figure 5(a) presents the temperature dependence of the real part of the dielectric constant measured at 1 MHz for $x=0.05$ – 0.10 in $(\text{Zr}_x\text{Ta}_{1-x})_2\text{O}_{5-x}$. The dielectric constant and $\tan\delta$ measured at varying frequencies are shown in Fig. S5 in the [supplementary material](#). With increasing ZrO_2 content, the dielectric constant at 30°C rises from 42 for $x=0.05$ to 50 for $x=0.10$. The dielectric constant exhibits a temperature dependence, reaching a maximum value at the specific temperature associated with the phase transition from $\text{L}'\text{-Ta}_2\text{O}_5$ to $\text{L}''\text{-Ta}_2\text{O}_5$.¹⁹ Figure 5(b) shows the compositional dependence of the phase transition temperatures determined from the maximum value of the dielectric constant displayed in Fig. 5(a). The phase transition temperature decreased linearly from 370°C for $x=0.05$ to 100°C for $x=0.10$ with increasing ZrO_2 content, corresponding to a reduction of $\sim 50^\circ\text{C}$ for each 0.01 increment in x .

C. Negative thermal expansion

Synchrotron HTXRD measurements were conducted at SPring-8 (BL13XU, $\lambda=0.375695\text{ nm}$) to investigate the temperature evolution of the $\text{L}'\text{-Ta}_2\text{O}_5$ -type phase ($x=0.05$). This study examined a temperature range of -173 to 800°C , as shown in Fig. S6 in the [supplementary material](#). The phase transition temperature for the transformation of the $\text{L}'\text{-Ta}_2\text{O}_5$ into the $\text{L}''\text{-Ta}_2\text{O}_5$ phase, determined from the HTXRD data, is $\sim 427^\circ\text{C}$ for $x=0.05$. By contrast, a previous study reported a transition temperature of 127°C for $x=0.10$.¹⁹ This indicates that samples with a lower ZrO_2 substitution exhibit a higher phase transition temperature, consistent with the findings from dielectric constant measurements.

The obtained lattice parameters are shown in Fig. 6 and data values including errors are shown in Table S2 in the [supplementary material](#). The data for $x=0.05$ are represented by red circles, while the data for $x=0.10$ are plotted as black squares for reference.¹⁹ For the samples with $x=0.05$, the parameter b increases, while the parameters a and c decrease up to 400°C . Above this temperature, all parameters gradually increase. Therefore, the phase transition temperature is estimated to be approximately 427°C based on HTXRD measurements. The observed difference of about 50°C in phase transition temperature between dielectric constant and HTXRD measurements arises from the distinct phenomena each technique detects. Dielectric constant measurements are highly sensitive to polarization fluctuations, whereas XRD measurements detect changes in the average crystal structure. Since polarization fluctuations become apparent before structural changes, the phase transition temperature

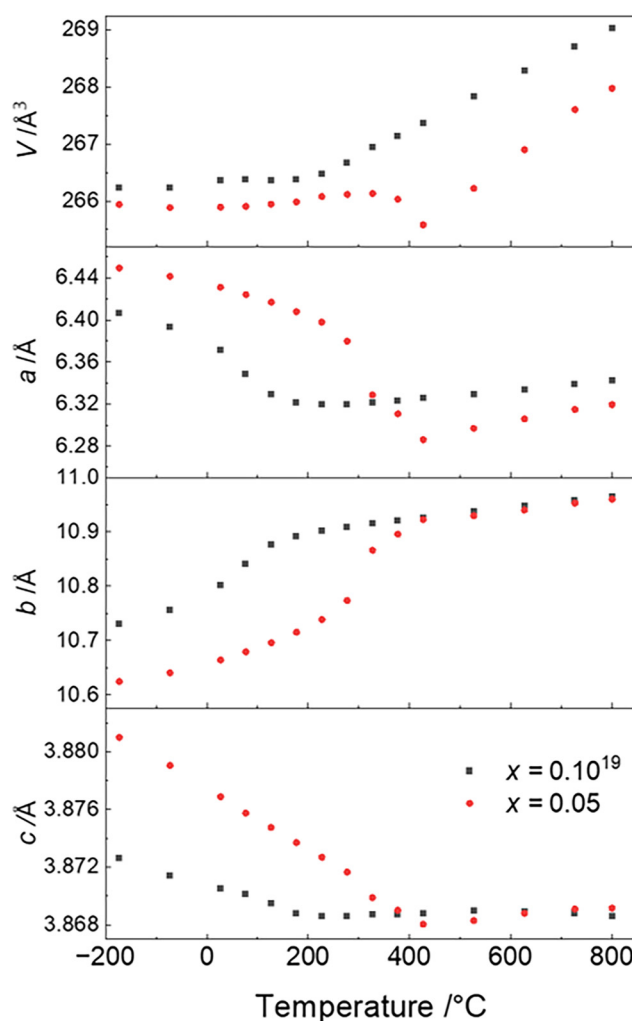


FIG. 6. Temperature dependence of the unit-cell volume and lattice parameters for $(\text{Zr}_x\text{Ta}_{1-x})_2\text{O}_{5-x}$ ($x=0.05$ and 0.10). The filled red circles and black squares represent the data for compositions of $x=0.05$ and 0.10 , respectively. The errors are within the circle and square data points.

determined by dielectric constant measurements tends to be lower than that determined by XRD.

The lattice volume decreases between 327 and 427°C in the vicinity of the phase transition temperature, indicating negative volumetric thermal expansion (NTE). Here, the volumetric thermal expansion coefficient, α_v , was calculated as $\alpha_v = \left(\frac{1}{V_0}\right) \left(\frac{V-V_0}{T-T_0}\right)$, where T represents the final temperature, T_0 the initial temperature, and the corresponding volumes are V and V_0 , respectively. At $x=0.05$, α_v was calculated to be $-2.06 \times 10^{-5}/\text{K}$ from the lattice volumes V_0 and V at 327 and 427°C in Table S2 in the [supplementary material](#). This value is comparable to that of ZrW_2O_8 , a well-known NTE material with $\alpha_v = -2.7 \times 10^{-5}/\text{K}$.²³

12 March 2026 00:17:58

For $x = 0.10$, the thermal expansion coefficient α_v was $-1.09 \times 10^{-6}/\text{K}$ in the temperature range of 77–127 °C. The sample with $x = 0.05$ had a wider NTE temperature range than $x = 0.10$ along with a larger thermal expansion coefficient.¹⁹ The unit-cell volume significantly shrinks before the phase transition from L' -Ta₂O₅ to L'' -Ta₂O₅ when the amount of ZrO₂ substitution is low. Uniquely, the NTE temperature range of the L' -Ta₂O₅ type (Zr_xTa_{1-x})₂O_{5-x} varied by ~200 °C (~473 K) through composition control, making it a promising candidate material for negative thermal expansion applications.

V. CONCLUSION

In this study, we investigated the formation process and composition-dependent properties of L' -Ta₂O₅ type (Zr_xTa_{1-x})₂O_{5-x}. HTXRD measurements indicated that the mixture of starting materials, ZrO₂ and Ta₂O₅, formed the H-Ta₂O₅ phase upon heating above 1360 °C. As the H-Ta₂O₅ phase cooled, it changed into the L'' -Ta₂O₅ phase, followed by the formation of the L' -Ta₂O₅ phase. A single-phase L' -Ta₂O₅ was obtained within the composition range of $x = 0.05$ –0.11. The material properties depended on the composition in the following ways:

- The lower the amount of ZrO₂ substitution, the slower the phase transition from the H-Ta₂O₅ phase to the L'' -Ta₂O₅ phase, making the H-Ta₂O₅ phase more likely to be quenched.
- With increasing extent of ZrO₂ substitution, the lattice parameters a and c increase, while b decreases.
- The dielectric constant at 30 °C increases with increasing extent of ZrO₂ substitution, ranging from $\epsilon_r = 42$ to 50. The temperature dependence of the dielectric constant revealed a maximum that corresponds to the phase transition from L' -Ta₂O₅ to L'' -Ta₂O₅. This transition temperature decreases by ~50 °C for every 0.01 increase in x .
- The L' -Ta₂O₅ phase shows NTE behavior near the phase transition temperature. Specifically, as the extent of ZrO₂ substitution decreases, the negative volume expansion coefficient increases. For the $x = 0.10$ sample, the thermal expansion coefficient, α_v , in the 77–127 °C range is $-1.09 \times 10^{-6}/\text{K}$, and for the $x = 0.05$ sample, α_v is $-2.06 \times 10^{-5}/\text{K}$ in the 327–427 °C range.

In conclusion, (Zr_xTa_{1-x})₂O_{5-x} ($x = 0.05$ –0.10), which forms the L' -Ta₂O₅ phase, is a material that allows for control over the dielectric constant, phase transition temperature, and thermal expansion behavior based on its composition.

SUPPLEMENTARY MATERIAL

See the [supplementary material](#) for the predicted phase transition pathway to the L' -Ta₂O₅ phase from the starting materials of ZrO₂ and L-Ta₂O₅, SHG signals for (Zr_xTa_{1-x})₂O_{5-x} ($x = 0.05$ –0.11), temperature dependence of HTXRD profiles of (Zr_{0.10}Ta_{0.90})₂O_{4.90}, lattice parameters with error bars for samples with x values ranging from 0.05 to 0.13 as well as for $x = 0.05$ and 0.10 during HTXRD measurements, and temperature dependence of real part of the dielectric constant for (Zr_xTa_{1-x})₂O_{5-x} ($x = 0.05$ –0.10) and raw synchrotron XRD data of (Zr_{0.05}Ta_{0.95})₂O_{4.95}.

ACKNOWLEDGMENTS

The authors thank Dr. Shintaro Kobayashi, Dr. Shogo Kawaguchi, and facility members at Japan Synchrotron Radiation Research Institute (JASRI) for the help with the SXRD experiments. The SXRD experiments were conducted at the BL13XU beamline at SPring-8 with the approval of JASRI (Proposal No. 2024B1693). This study was partly supported by Japan Society for the Promotion of Science (JSPS) KAKENHI, Grant Nos. JP23H02050, JP23K26743, and JP25K17643, research granted from Murata Science and Education Foundation, and from the Yoshishige Abe Memorial Fund.

AUTHOR DECLARATIONS

Conflict of Interest

The authors have no conflicts to disclose.

Author Contributions

Suzuka Udagawa: Conceptualization (lead); Investigation (lead); Visualization (lead); Writing – original draft (lead); Writing – review & editing (equal). **Takanori Mimura:** Conceptualization (equal); Funding acquisition (equal); Investigation (equal); Supervision (equal); Writing – original draft (equal); Writing – review & editing (equal). **Tetsuhiro Katsumata:** Investigation (equal); Writing – review & editing (supporting). **Yoshitaka Matsushita:** Investigation (supporting); Writing – review & editing (supporting). **Takashi Mochiku:** Investigation (supporting); Writing – review & editing (supporting). **Yoshiyuki Inaguma:** Funding acquisition (equal); Investigation (equal); Supervision (equal); Writing – original draft (equal); Writing – review & editing (equal).

DATA AVAILABILITY

The data that support the findings of this study are available from the corresponding author upon reasonable request.

REFERENCES

- R. J. Cava, *J. Mater. Chem.* **11**(1), 54–62 (2001).
- R. M. Wallace and G. D. Wilk, *Crit. Rev. Solid State Mater. Sci.* **28**(4), 231–285 (2003).
- M. Ghevondyan, M. Davtyan, and M. Aghayan, *Discov. Mater.* **5**, 43 (2025).
- K. Zhang, L. Chao, and J. Zhou, *Materials* **11**(8), 1332 (2018).
- Q. Li, F.-Z. Yao, Y. Liu, G. Zhang, H. Wang, and Q. Wang, *Annu. Rev. Mater. Res.* **48**(1), 219–243 (2018).
- J. P. B. Silva, K. C. Sekhar, H. Pan, J. L. MacManus-Driscoll, and M. Pereira, *ACS Energy Lett.* **6**(6), 2208–2217 (2021).
- H.-F. Zhang, B.-Y. Ning, T.-C. Weng, and X.-J. Ning, *J. Am. Ceram. Soc.* **104**(12), 6413–6423 (2021).
- M. Hiratani, S. Kimura, T. Hamada, S. Iijima, and N. Nakanishi, *Appl. Phys. Lett.* **81**(13), 2433–2435 (2002).
- F. Rubio, J. Denis, J. M. Albella, and J. M. Martinez-Duart, *Thin Solid Films* **90**(4), 405–408 (1982).
- L. Waring and R. S. Roth, *J. Res. Natl. Bur. Stand. A Phys. Chem.* **72A**, 175–186 (1967).
- G. L. Brennecke, D. A. Payne, P. Sarin, J. M. Zuo, W. M. Kriven, and H. Hellwig, *J. Am. Ceram. Soc.* **90**(9), 2947–2953 (2007).
- X. Q. Liu, X. D. Han, Z. Zhang, L. F. Ji, and Y. J. Jiang, *Acta Mater.* **55**(7), 2385–2396 (2007).

12 March 2026 00:17:58

- ¹³N. C. Stephenson and R. S. Roth, *Acta Crystallogr. B* **27**(5), 1037–1044 (1971).
- ¹⁴R. J. Cava, J. J. Krajewski, W. F. Peck, Jr., and G. L. Roberts, *J. Appl. Phys.* **80**(4), 2346–2348 (1996).
- ¹⁵R. J. Cava and J. J. Krajewski, *J. Appl. Phys.* **83**(3), 1613–1616 (1998).
- ¹⁶Y. Wang and Y.-J. Jiang, *Mater. Sci. Eng. B* **99**(1–3), 221–225 (2003).
- ¹⁷R. F. Cava, W. F. Peck, Jr., and J. J. Krajewski, *Nature* **377**(6546), 215–217 (1995).
- ¹⁸D. Makovec, J. M. Zuo, R. Twisten, and D. A. Payne, *J. Solid State Chem.* **179**(6), 1782–1791 (2006).
- ¹⁹T. Mimura, S. Udagawa, and Y. Inaguma, *Appl. Phys. Lett.* **126**(15), 151902 (2025).
- ²⁰Y. Inaguma, A. Aimi, D. Mori, T. Katsumata, M. Ohtake, M. Nakayama, and M. Yonemura, *Inorg. Chem.* **57**(24), 15462–15473 (2018).
- ²¹P. Luo, X. Wu, W. Xiao, F. Zhang, Y. Wang, D. Huang, and Y. Du, *J. Am. Ceram. Soc.* **105**(1), 668–686 (2022).
- ²²A. Le Bail, H. Duroy, and J. L. Fourquet, *Mater. Res. Bull.* **23**(3), 447–452 (1988).
- ²³J. S. O. Evans, T. A. Mary, T. Vogt, M. A. Subramanian, and A. W. Sleight, *Chem. Mater.* **8**(12), 2809–2823 (1996).